The h-SbxWO3+2x Oxygen Excess Antimony Tungsten Bronze

von Rohr, Fabian O ; Ryser, Alice ; Ji, Huiwen ; Stolze, Karoline ; Tao, Jing ; Frick, Jessica J ; Patzke, Greta R ; Cava, Robert J

Abstract: We describe the previously unreported oxygen excess hexagonal antimony tungsten bronze with composition Sb0.5W3O10, in the following denoted as h-SbxWO3+2x with x=0.167, to demonstrate its analogy to classical AxWO3 tungsten bronzes. This compound forms in a relatively narrow temperature range between 580 °C<T<620 °C. It was obtained as a dark-blue polycrystalline powder, and as thin, needle-shaped, blue single crystals. h-SbxWO3+2x crystallizes in the hexagonal space group P6/mmm with the cell parameters a=7.4369(4) Å and c=3.7800(2) Å. The antimony and excess oxygen occupy the hexagonal channels within the network of corner-sharing WO6 octahedra. h-SbxWO3+2x has a resistivity of 300 K 1.28 mΩ cm at room temperature, with little if any temperature-dependence on cooling. DFT calculations on a simplified model for this compound find a metallic-like electronic structure with the Fermi level falling within rather flat bands, especially around the Γ point.

DOI: https://doi.org/10.1002/chem.201805251

The *h*-Sb_xWO_{3+2x} Oxygen Excess Antimony Tungsten Bronze

Fabian O. von Rohr,[*,†] Alice Ryser,[‡] Huiwen Ji,[‡] Karoline Stolze,[‡] Jing Tao,[¶] Jessica J. Frick,[‡] Greta R. Patzke,[†] and Robert J. Cava[‡]

†*Department of Chemistry, University of Zurich, CH-8057 Zurich, Switzerland*

‡*Department of Chemistry, Princeton University, Princeton, New Jersey 08544, USA*

¶*Condensed Matter Physics Department, Brookhaven National Laboratory, Upton, New York 11973, USA*

E-mail: fabian.vonrohr@chem.uzh.ch

Abstract

We describe the previously unreported oxygen excess hexagonal antimony tungsten bronze with composition $Sb_{0.5}W_3O_{10}$, in the following denoted as *h*-Sb_xWO_{3+2x} with $x = 0.167$, to demonstrate its analogy to classical A_xWO_3 tungsten bronzes. This compound forms in a relatively narrow temperature range between 580 °C $< T <$ 620 °C. It was obtained as a dark-blue polycrystalline powder, and as thin, needle-shaped, blue single crystals. *h*-Sb_xWO_{3+2x} crystallizes in the hexagonal space group $P6/mmm$ with the cell parameters $a = 7.4369(4)$ Å and $c = 3.7800(2)$ Å. The antimony and excess oxygen occupy the hexagonal channels within the network of corner-sharing WO_6 octahedra. *h*-Sb_xWO_{3+2x} has a resistivity of $\rho_{300K} \approx 1.28$ mΩ cm at room temperature, with little if any temperature-dependence on cooling. DFT calculations on a simplified model for this compound find a metallic-like electronic structure with the Fermi-level falling within rather flat bands, especially around the Γ point.

Introduction

Tungsten bronzes are a large family of compounds based on three-dimensional networks of corner-sharing [WO_6] octahedra. These materials have been intensely studied for their potential applications in smart windows, chromogenic devices, sensors, dye-sensitized solar cells, and photoelectrochemical water splitting.[1–4] They are however, also of great interest in fundamental research due to their structural variety and because they can act as hosts for interesting physical properties such as superconductivity, magnetic ordering, and ferroelectricity.[5–11] Tungsten bronzes can generally be described as A_xWO_3 type phases, where an electropositive guest atom A is intercalated into cavities in the 3D WO_3 network. These phases crystallize in a number of different structures that can be classified into four groups depending on the geometry of the WO_3 network, namely: the perovskite tungsten bronze (PTB), the intergrowth tungsten bronze (ITB), the tetragonal tungsten bronze (TTB), and the hexagonal tungsten bronze (HTB).

The known tungsten bronzes in the Sb-W-O chemical system display a range of structural features. Tungsten bronze structures containing antimony are of particular interest from a structural and bonding point of view as in these compounds antimony can either be in a Sb(III) formal oxidation state, leading to the presence of a stereochemically active lone pair, or in a Sb(V) formal oxidation state, which is considered to be more stable, but less commonly encountered in oxides. Furthermore, antimony may form covalent bonds with the oxygen atoms in the network, which may lead to strong electronic interactions between the tungsten bronze host network and the antimony intercalant atoms. So far, two antimony tungsten bronzes containing Sb(III) have been reported: (i) For low antimony contents in Sb_xWO_3 ($x \leq 0.07$), perovskite type bronzes form, with the antimony metal atoms in the cages between the WO_6 octahedra in the parent WO_3 structure.[12] This is analogous to the low intercalant concentration alkali tungsten bronzes, and also to the bronzes found for the other group 15 metals arsenic and bismuth.[13] (ii) Additionally, an ITB phase is known in

the system Sb-W-O, which is i-Sb_xWO_3 with $0.12 \leq x \leq 0.20$. This ITB crystallizes in the orthorhombic space group *Pmmm* (No. 47).[14] Its framework includes hexagonal channels, which are occupied by the antimony atoms. These channels are separated by perovskite-type slabs (along the *b*-direction) that are two WO_6-octahedra wide. The $[WO_3]$-framework of the i-Sb_xWO_3 can be considered the simplest of all possible frameworks for ITB phases, since it has the minimal perovskite-like WO_3-type slab thickness possible for an ITB. *Klingstedt et al.* combined exit-wave reconstruction from focal series of HRTEM images with single crystal XRD and total energy studies on this ITB.[15] They found an improved structure refinement with the incorporation of oxygen covalently bound to antimony in the tunnels for a certain stoichiometry, similar to what has been reported for the HTB-like phase encountered in the Sb-Mo-O system.[16]

Here we describe the previously unreported oxygen-excess hexagonal antimony tungsten bronze. Our studies clearly show that this material contains $[SbO_2]^+$ units, which establishes this compound as the first tungsten bronze with antimony in a formal Sb(V) oxidation state. The discovery of this hexagonal tungsten bronze bridges a logical deficiency in the structural chemistry of antimony tungsten bronzes, extending the structures of the known perovskite-type and intergrowth bronzes in the Sb-W-O system. Furthermore, it establishes the structural richness of the Sb-W-O chemical system.

Results and Discussion

Synthesis and single crystal x-ray diffraction. Powder xray diffraction indicated the presence of a hexagonal bronze in the Sb-W-O system, and detailed phase equilibria studies performed to determine the composition of the hexagonal bronze phase clearly indicated it to form at one particular antimony content, and, critically, only with an excess oxygen content equal to the amount of twice the antimony present. The compound with the composition

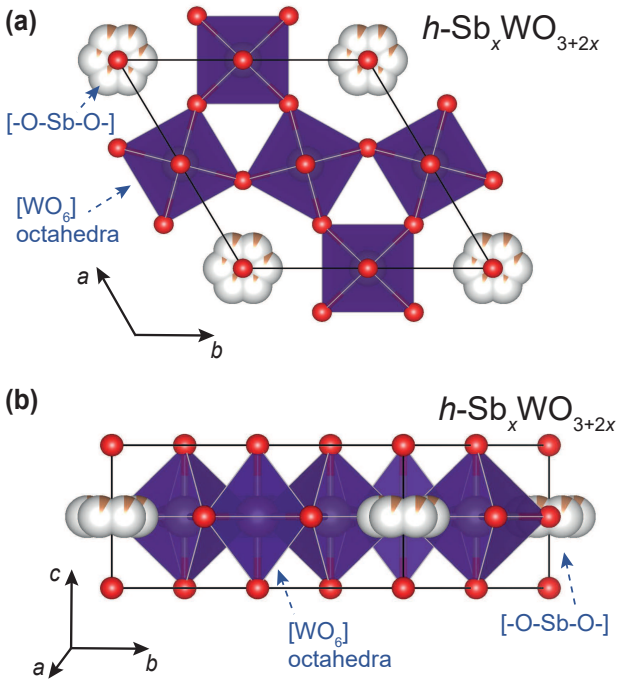

Figure 1: Crystal structure of h-Sb_xWO_{3+2x} along the (a) c-direction and a high-symmetry (b) ab direction. The crystal structure was obtained by a single crystal XRD structural refinement (for details of the refinement, see tables 1-3). The oxygen atoms are red, and the $[WO_6]$ octahedra purple. The partially occupied antimony positions are orange/white. In h-Sb_xWO_{3+2x}, each antimony site is split into 6 partially occupied off-center positions that sum to a antimony atom occupancy of $x = 0.167$.

$Sb_{0.5}W_3O_{10}$ - in the following denoted as h-Sb_xWO_{3+2x} with $x = 0.167$, according to common practice for tungsten bronzes - was obtained as a single phase polycrystalline dark-blue powder, and, eventually as blue needle-shaped single crystals from the LiCl mixture. The samples were found to be stable in air and moisture. The crystal structure of h-Sb_xWO_{3+2x} was solved and refined from single-crystal XRD data in the hexagonal space group $P6/mmm$ (No. 191) with $a = 7.4369(4)$ Å and $c = 3.7800(2)$ Å. We did not let the occupation of antimony relax freely in the single crystal refinement process, since such a procedure would not converge due to the positional and vibrational disorder associated with the antimony. Instead, the other parameters were first refined, and the antimony occupation was manually changed with a small step width (the corresponding the R_1 and wR_2 values are shown in the Supplemental Information accordingly). The antimony content was held constant according to the Sb:W ratio of 0.167:1, which corresponds to a stoichiometric $[SbO_2]^+$ unit in the channels. This is in agreement with the fine-tuned refinements, and within error of the obtained antimony to tungsten ratio of 0.170:1.00 from our ICP-MS elemental analysis. The details of the refinement are summarized in table 1, and the corresponding crystallographic positions are presented in table 2. The anisotropic displacement parameters for tungsten and antimony are listed in table 3.

The unit cell of the refined structure for h-Sb_xWO_{3+2x} is depicted in figure 1 along the c-axis and along a high-symmetry crystallographic axis in the ab-direction. The crystal structure of h-Sb_xWO_{3+2x} is closely related to other hexagonal tungsten bronzes. The antimony is not in the ideal central position $(0,0,\frac{1}{2})$ in the tunnel that corresponds to the Wyckoff position $1b$. We rather find a strongly improved convergence of the structural model with the experimental single-crystal XRD data when the antimony is split into 6 partially occupied positions $(0;y;\frac{1}{2})$ displaced from the center of the tunnels, corresponding to the Wyckoff position $6k$. Only one of the displaced positions can be occupied in any tunnel, because the displaced sites are too close together to accommodate more than a single Sb.

Table 1: Details of the single-crystal x-ray diffraction measurements and structural refinement for h-Sb_xWO_{3+2x}.

Parameters	h-$Sb_{0.167}WO_{3.33}$
Composition	$Sb_{0.5}W_3O_{10}$
Crystal system	hexagonal
Space group	*P6/mmm* (No. 191)
Absorption correction method	SADABS
Temperature	298 K
Lattice parameters [Å]	$a = 7.4369(4)$
	$c = 3.7800(2)$
Cell volume [Å]^3	181.05(2)
Formula units/cell	1
ρ_{cal} [g cm^{-3}]	7.084
μ [mm^{-1}]	49.325
Crystal size [mm]	0.007 x 0.014 x 0.048
F(000)	327.5
Radiation type	Mo $K\alpha_1$ $\lambda = 0.71073$
Θ range [°]	3.163 - 27.472
Index ranges	h [-8, 9]
	k [-9, 9]
	l [-4, 4]
Observed reflections	2563
Independent reflections ($\geq 2\sigma$)	109
R_{int}	0.0135
R_σ	0.0390
Refined parameters	17
GOF	1.356
R_1 (all data)	0.0148
R_1 ($\geq 2\sigma$)	0.0148
wR_2 (all data)	0.0346
wR_2 ($\geq 2\sigma$)	0.0346
Max/min residual electron density [e Å^3]	0.708/-1.313

Table 2: Atomic coordinates, isotropic displacement parameters, and occupancies of the atoms in h-Sb_xWO_{3+2x}, in space group *P6/mmm* at ambient temperature, and their isotropic thermal displacement parameters. The unit cell dimensions are [Å] $a = 7.4369(4)$ and $c = 3.7800(2)$.

Atom	Wyckoff symbol	x	y	z	U_{iso} [Å^2]	*Occ.*
W	$3g$	1/2	0	1/2	0.0103(14)	1
Sb	$6k$	0	0.0841(9)	1/2	0.031(3)	0.083
O1	$3f$	1/2	0	0	0.0074(16)	1
O2	$6m$	0.4221(8)	0.2111(4)	1/2	0.0094(19)	1
O3	$1a$	0	0	0	0.0111(19)	1

Table 3: Anisotropic displacement parameters [Å^2] of tungsten and antimony in h-Sb_xWO_{3+2x}. Anisotropic displacement parameters of the oxygen atoms were not refined in order to obtain an improved data-to-parameter ratio.

Atom	U_{11}	U_{22}	U_{33}	U_{12}
W	0.0169(14)	0.0055(14)	0.0045(15)	0.0028(7)
Sb	0.022(6)	0.009(3)	0.067(5)	0.011(3)

The sum of the occupancies leads to a total Sb content of $x = 0.167$, which corresponds to the occupancy of Sb in every other hexagonal cavity position in the tunnel. The absence of a superlattice indicates that there is no long range order of the Sb in the cavities. Thus, in this compound, antimony is found to occupy channels within the hexagonal bronze network of WO_6 octahedra, being surrounded by a total of six oxygen atoms. Four oxygen atoms are in a plane around an antimony atom, while the other two oxygen atoms are in the polar positions. The displacement of the Sb from the center of the cavity allows it to optimize its bond lengths to oxygen: the Sb-O bond lengths are 2 x 1.99 Å and 2 x 2.20 Å to nearby oxygens and 2 x 2.78 Å and 2 x 3.28 Å to oxygens across the hexagonal cavity, consistent with reported values for other oxides. The corresponding network of polyhedra for h-Sb_xWO_{3+2x} viewed along the c-axis is shown in figure 2a, and the details of the coordination polyhedra of the distorted [SbO_8] hexagonal bipyramid and the WO_6 octahedra with the corresponding metal-oxygen bond lengths are depicted in figure 2(b)-(c). The inclusion of excess O in the hexagonal bronze channels is at first unexpected, but earlier reports showed that Sb_2O units

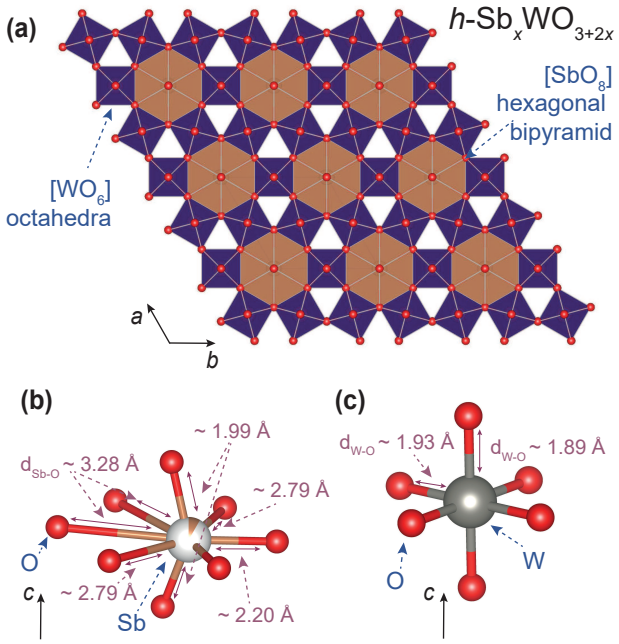

Figure 2: (a) The polyhedral representation of h-Sb_xWO_{3+2x}, showing the network consisting of $[WO_6]$ octahedra, and also of distorted $[SbO_8]$ hexagonal bipyramids. Coordination polyhedra of (b) the distorted $[SbO_8]$ hexagonal bipyramid and the (c) WO_6 octahedra with the corresponding metal-oxygen bond lengths.

are in the channels in the Sb-Mo-O for one of the ITB phases[16] and Sb-O-Sb bonding was discussed as being potentially present in the ITB in the Sb-W-O system.[15] The current work is the first to characterize the Sb-O system within the tunnels.

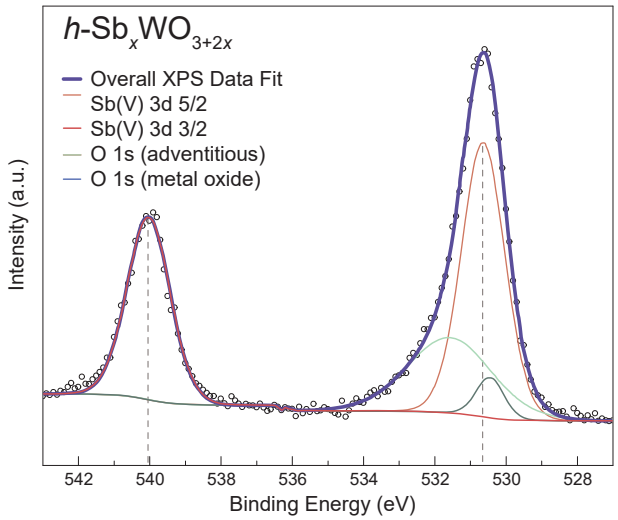

Figure 3: Representative XPS spectrum of single crystals of h-Sb_xWO_{3+2x}. The overall (blue line) and deconvoluted fits of the raw data (black circle) for the Sb(V) 3d 5/2 (orange line), the Sb(V) 3d 3/2 (red line), adventitious oxygen 1s transitions (light green line), and the oxygen 1s from the metal-oxygen bond (green line) transitions are shown. The agreement of the data with an assignment of an Sb(V) oxidation state is excellent.

X-ray photoelectron spectroscopy. The composition $Sb_{0.5}W_3O_{10}$, as obtained from SXRD measurements, along with the blue color and metallic conductivity of the material, indicates the presence of antimony in the oxidation state Sb(V) in h-Sb_xWO_{3+2x}. An Sb(III) oxidation state is incompatible with the formula of the compound and its transport properties; it would for example lead to a tungsten oxidation state of greater than +6, which is not possible under our conditions and to electrically insulating behavior, which is not observed. However, because the presence of the Sb(V) state can be considered unexpected, we verified the exclusive presence of antimony with the oxidation state Sb(V) in this compound by x-ray photoelectron spectroscopy (XPS). No antimony in the oxidation state Sb(III) was detected; only Sb(V) was present. In figure 3 the XPS spectrum obtained between 525 and 543 eV for single crystals is shown. The observed peaks at energies of $E_1 = 530.6$ eV and $E_1 = 540.0$ eV correspond to the Sb(V) 3d 5/2 and the Sb(V) 3d 3/2 transitions, respectively. The fits of the raw data for the Sb(V) 3d 5/2 (orange line), the Sb(V) 3d 3/2 (red line), adventitious oxygen 1s transitions (light green line), and the oxygen 1s from the metal-oxygen bond (green line) transitions are depicted individually in figure 3. As can be seen, the oxygen

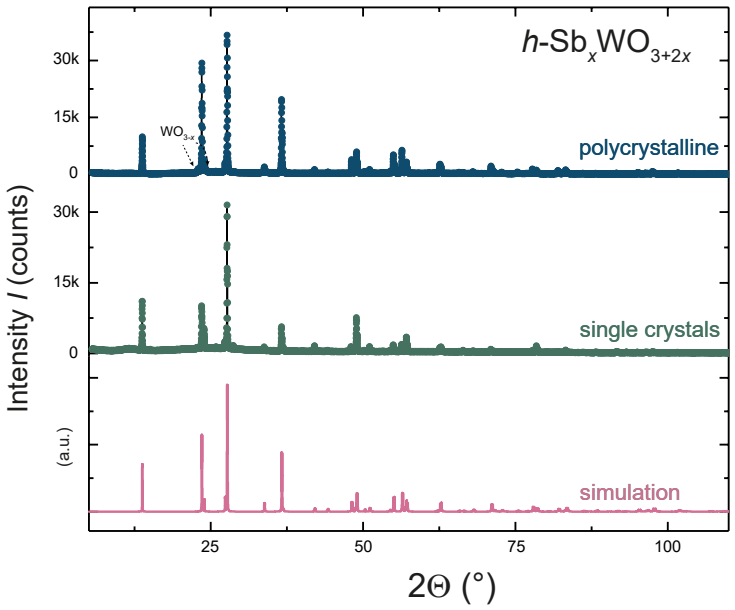

Figure 4: Powder x-ray diffraction pattern measured on a polycrystalline sample and a sample of crushed single crystals of h-Sb$_x$WO$_{3+2x}$. For reference the simulated PXRD pattern obtained from the single crystal XRD refinement is also shown.

peaks can be fully separated from the antimony peaks, when making use of the Sb(V) 3d 3/2 transition at the higher binding energy (for further details on the oxidation state assignment of antimony, refer to reference 17). The fit (emphasized blue line) for both the Sb(V) 3d 5/2 and the Sb(V) 3d 3/2 transitions is excellent, unambiguously confirming the oxidation state of Sb(V) in this compound.

Powder x-ray diffraction. In figure 4, the powder x-ray patterns (PXRD) measured on a polycrystalline sample and on a sample of crushed single crystals of h-Sb$_x$WO$_{3+2x}$ are depicted. In the bottom panel the simulated PXRD pattern from the single crystal XRD refinement is shown for reference. Both PXRD patterns are in good agreement with the simulated diffraction pattern, thereby verifying the validity of the obtained structural model. Polycrystalline h-Sb$_x$WO$_{3+2x}$ proved to be challenging to synthesize as a single phase. Firstly, for a synthesis at low temperatures ($T < 600$ °C), we found that WO_3, WO_2, or mixtures of WO_{3-x} were still present after the reaction appeared to stop. Secondly, at higher

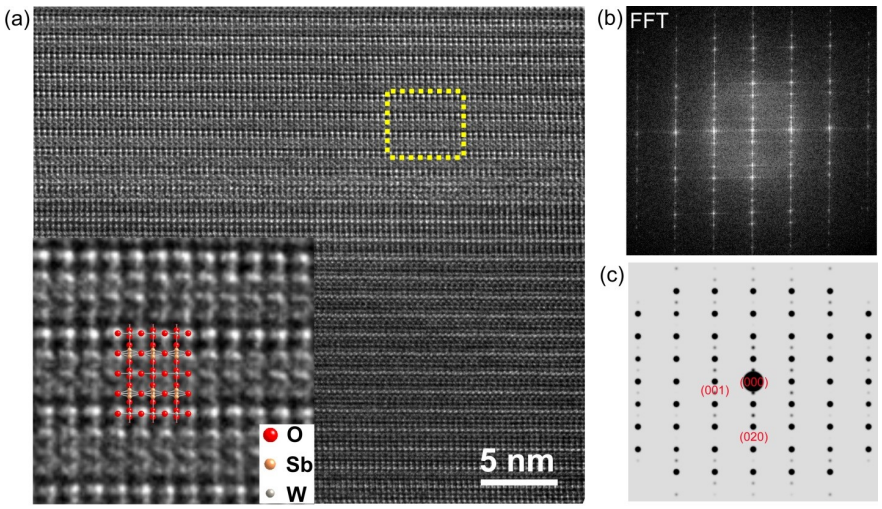

Figure 5: (a) High-resolution TEM (HRTEM) image of single-crystal h-Sb_xWO_{3+2x} with the a-axis perpendicular to the image plane. Boxed area was enlarged and shown at the bottom-right corner, with its atomic structure superposed on the image. (b) The Fast Fourier Transform of the HRTEM image of (a), which is consistent with the kinematic electron diffraction simulation at the [100] zone axis (shown in (c)) using the crystal structure demonstrated in figure 1.

temperature ($T > 620$ °C), the ITB i-Sb_xWO_3 was found to be the thermodynamically most stable phase. Thirdly, we found that this oxide is very sensitive to having the correct oxygen content present - only syntheses with the precise stoichiometry of h-$Sb_{0.167}WO_{3.33}$ resulted in samples with an acceptably low amount of impurity present. The optimal synthesis conditions were found to be 600 °C for 12 h, the resulting PXRD pattern from this synthesis contains only minor impurity peaks of WO_{3-x}, as shown in figure 4.

Transmission electron microscopy. In figure 5(a), we show a high-resolution TEM image (HRTEM) obtained from single-crystal h-Sb_xWO_{3+2x}, manifesting a good crystalline structure in a large area. The corresponding Fast Fourier Transform (FFT) of the HRTEM image in figure 5(b) is consistent with the simulated kinematic electron diffraction pattern (figure 5(c)) based on the crystal structure shown in figure 1. The consistency between the FFT of the HRTEM image and simulated kinematic electron diffraction supports the atomic model presented here.

Physical properties. In figure 6, we show the resistivity of a polycrystalline pellet

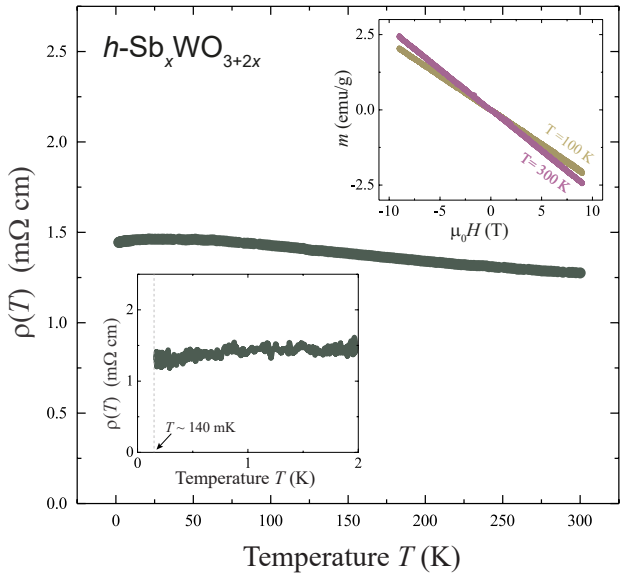

Figure 6: Temperature-dependent resistivity of h-Sb_xWO_{3+2x} in the temperature range between T = 300 K and 140 mK. Lower left inset: Resistivity in the very low temperature region between T = 140 mK and 2 K. Upper right inset: Field-dependent magnetization of h-Sb_xWO_{3+2x} at 100 K and 300 K, for applied fields between $\mu_0 H$ = -9 T and +9 T.

of h-Sb_xWO_{3+2x} in the temperature range between T = 300 K and 140 mK. Unlike the case for many hexagonal tungsten bronzes, no transition to a superconducting state is observed. The resistivity at room temperature is $\rho_{300\mathrm{K}} \approx 1.28$ mΩ, and the resistivity does not decrease with decreasing temperature. This "poor metal" or semimetallic behavior, as commonly observed for polycrystalline samples of compounds with a low density of electronic states at the Fermi-level,[18] where grain-boundary scattering is significant compared to the low intrinsic conductivity, is particularly often observed for polycrystalline samples of metallic oxides (see, e.g., references 19–21). In the inset on the lower left of figure 6, we show the resistivity between T = 140 mK and 2 K. (The increased noise of the measured signal is caused by the small current of only 10 nA that is applied for these measurements, used to avoid self-heating of the sample.) No transition to a superconducting state can be observed down to a temperature of T = 140 mK. In the inset of the upper right corner of figure 6, we

show the field-dependent magnetizations of a polycrystalline pellet of h-Sb_xWO_{3+2x} at T = 100 K and 300 K. The material is weakly diamagnetic, consistent with it having a very low density of electronic states at E_F and significant core diamagnetism (due to the W present).

Electronic structure. In order to get further insight into the poor metallic behavior, the apparently low density of electronic states observed, and the absence of superconductivity, electronic structure calculations were performed for a model of the material. The model places Sb in the center of the hexagonal cavity and in an ordered array (i.e. a 2x superlattice) within the cavities, and thus is not expected to describe the electronic system in detail, but rather provides a general picture of the electronic state of the material. In figure 7(c), we show the calculated electronic density of states within (a) 10 eV and (b) 2 eV of the Fermi level (E_F). In figure 7, we show the resulting calculated electronic band structure of h-Sb_xWO_{3+2x}. The high-symmetry $\vec{k}$-path in the Brillouin zone was chosen for a hexagonal unit cell. From the calculated electronic density of states and the electronic band structure, we can conclude that h-Sb_xWO_{3+2x} is an intrinsic metal. The Fermi-level appears to lie at the bottom of a broad conduction band within which relatively localized states are also found. A relatively small amount of occupied states is found at the Fermi-level. The resemblance of this electronic band structure to that of the conventional alkali-based hexagonal tungsten bronzes A_xWO_3 (A = Rb, K) becomes evident upon comparison.[22] Also the overall resistivities are in good agreement with the alkali intercalated tungsten bronzes. From a chemist's perspective this can be explained by two reasons: Firstly, all three of these hexagonal tungsten bronzes are structurally similar, and secondly K^+, Rb^+, and $[SbO_2]^+$, with antimony in a Sb(V) oxidation state, formally contribute the same number of electrons to the hexagonal WO_3 framework. However, in contrast to the h-$Sb_{0.167}WO_{3.33}$ HTB reported here, the $A_{0.16}WO_3$ hexagonal bronzes are known superconductors with critical temperatures of T_c between $\approx$ 3 K, and 4 K.[22–24] The absence of superconductivity in h-Sb_xWO_{3+2x} is therefore rather surprising at first. It may be caused by differences in the phonon-spectra

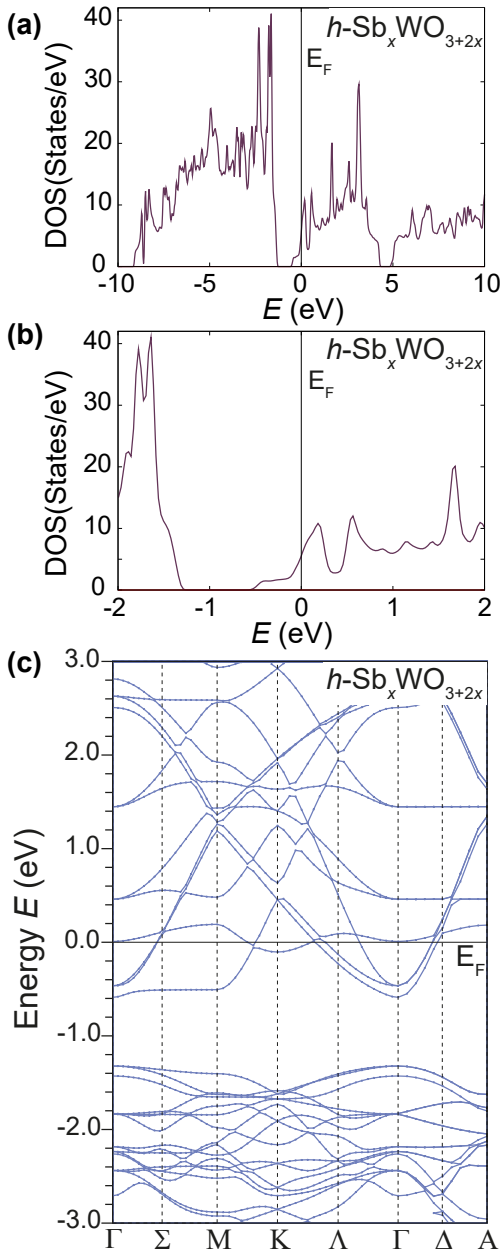

Figure 7: Electronic structure of h-Sb_xWO_{3+2x}: (a) Calculated electronic density of states from -10 eV to +10 eV and (b) in the vicinity of the Fermi-level for a model of the hexagonal oxygen excess antimony tungsten bronze (c) Band structure of h-Sb_xWO_{3+2x} along a hexagonal $\vec{k}$-path. For details of the calculation see text.

between the alkali and antimony variants, or by disruption of the critical electronic properties of the system by the presence of a small amount of antimony orbital character at E_F or the oxygen in the cavities, although a significant number of the conventional alkali tungstate bronzes are superconducting. Based on empirical observations, we speculate that it may be possible to induce superconductivity in h-Sb_xWO_{3+2x} by either (i) electron doping of the compound towards the van-Hove singularity in the electronic density of states above E_F (see, e.g. reference 22), or (ii) by phonon-softening, e.g. if the compound can be chemically tuned towards a structural instability (see, e.g. references 25,26).

Summary and Conclusion

We have characterized a new compound in the Sb-W-O chemical system. The crystal structure of this compound was solved and refined by single-crystal x-ray diffraction. It crystallizes in the hexagonal space group $P6/mmm$ with the antimony and oxygen occupying hexagonal channels within a network of corner-sharing WO_6 octahedra. The antimony in the channels is displaced from the centers of the hexagonal cavities. Our XPS spectrum verifies the exclusive presence of antimony in the oxidation state Sb(V) in this compound. The crystal structure was further investigated by PXRD and high-resolution TEM, which clearly confirm the oxygen excess and the validity of the structural model derived from single-crystal x-ray diffraction. The discovery of this hexagonal tungsten bronze extends the structural series beyond the known perovskite type Sb_xWO_3 phase for low antimony contents and the known ITB phase. h-Sb_xWO_{3+2x} is found to be a poor metal with a resistivity at room temperature of $\rho_{300K} \approx 1.28$ mΩ cm. From the resistivity, diamagnetic susceptibility and electronic band structure, we find that h-Sb_xWO_{3+2x} should be a low density of states metal. The resistivity measured down to $T = 140$ mK does not show any signs of superconductivity or any other electronic transitions, which is in contrast to the electronic and structurally closely related hexagonal A_xWO_3 phases with A = Rb, and K, and suggests that the SbO_2 units present

disrupt the electronic or vibrational characteristics that lead to superconductivity in the alkali tungsten bronzes.

Experimental Section

Synthesis. The precursor WO_2 was prepared by heating WO_3 (99.998 %) in forming gas (95 % Ar/ 5 % H_2) at 700 °C for 12h. Polycrystalline samples of h-Sb_xWO_{3+2x} were synthesized by mixing Sb_2O_5 (99.998 %), WO_3 (99.998 %), and WO_2 in stoichiometric ratios. The total mass of each h-Sb_xWO_{3+2x} synthesis was 300 mg. The reactants were pressed in a pellet, placed in a corundum crucible, and sealed in an evacuated quartz glass tube. The reaction mixtures were heated to 600 ° C at a rate of 180 °C/h, where they were annealed for 12 h; the product was cooled to room temperature by quenching the evacuated quartz glass tubes in air.

Single crystals were obtained by sealing the polycrystalline h-Sb_xWO_{3+2x} powder with dry LiCl in a ratio of 1:20 in a 8 cm long evacuated quartz tube. The mixture was placed in a tube furnace at 600 °C. After ten days, thin, needle-shaped crystals were obtained at the cold end of the tube.

Structural characterization. Single crystal x-ray diffraction was performed using a Bruker D8 VENTURE diffractometer equipped with a Photon 100 CMOS detector, with Mo $K\alpha$ and a graphite monochromator (λ = 0.71073 Å) at room temperature. We did not observe any diffuse scattering (see Supporting Information). The unit cell determination and subsequent data collection, integration, and refinement were performed with the Bruker APEX II software package. The crystal structure was determined using SHELXL-2013 software implemented through the WinGX Suite. Powder x-ray diffraction (PXRD) patterns were obtained from finely ground samples on a Bruker D8 Advance Eco with copper $K\alpha$ radiation in a Bragg-Bretano geometry and a LynxEye-XE detector. Transmission electron

microscopy images were obtained at Brookhaven National Laboratory on a JEOL 3000F microscope equipped with a Gatan liquid-helium cooling stage. X-ray photoelectron spectra (XPS) were collected under a pressure of $p \approx 10^9$ Torr using a ThermoFisher K-Alpha X-ray photoelectron spectrometer. All spectra were recorded using Al $K\alpha$ radiation ($E = 1487$ eV) with a survey and pass energy of 100 and 20 eV, respectively. The C 1s peak at a binding energy of $E = 284.5$ eV of adventitious hydrocarbon was used as the internal binding energy reference. The elemental analysis was carried out by Mikroanalytisches Labor Pascher (Remagen, Germany).

Physical property measurements. The temperature-dependent resistivity and magnetization measurements were performed in a *Quantum Design* Physical Property Measurement System (PPMS). For the resistivity measurements, a standard 4-probe technique was employed using 25 μm diameter platinum wire bonded with silver paint. The resistivity was measured in the temperature range between $T = 300$ K to 140 mK. For temperatures above $T > 2$ K a current of $I = 1$ mA was applied, and for temperatures below $T < 2$ K, a current of 10 nA was applied. For the resistivity measurements between $T = 2$ K and 140 mK, the Adiabatic Demagnetization Refrigerator (ADR) option by *Quantum Design* was used. The field-dependent magnetization the vibrating sample magnetometer (VSM) option was used. Crushed, and finely ground single crystals were measured at $T = 100$ K and 300 K, respectively, in external fields between $\mu_0 H =$ -9 T and +9 T.

Band-structure calculations. The electronic band structure calculations were performed using density functional theory (DFT), via the WIEN2K code with a full-potential linearized augmented plane wave and local orbitals basis,[27–29] together with the Perdew-Burke-Ernzerhof parametrization of the generalized gradient approximation. The plane-wave cutoff parameter $R_{MT}K_{max}$ was set to 7, and the reducible Brillouin zone was sampled by 2000 k points; spin-orbit coupling was included. Due to the structural disorder present (the Sb ions

are disordered over a cluster of off-center sites in the tunnels) the structure was modelled by an artificial ordered supercell with $a_{supercell} = 3\ a_{subcell}$ and stoichiometry SbW_6O_{20}, with the antimony atoms placed in the ideal on-center (0;0;0.5) position (Wyckoff symbol 1*b*) of the hexagonal unit cell.

Acknowledgments

This work was supported by the University of Zurich, by the Swiss National Science Foundation under Grant No. PZ00P2_174015, and by the US Department of Energy, Division of Basic Energy Sciences, grant DE-FG02-98ER45706. The work at Brookhaven was sponsored by the U.S. DOE BES, by the Materials Sciences and Engineering Division under Contract DE-SC0012704, and supported by the resources of the Center for Functional Nanomaterials at Brookhaven National Laboratory, which is a U.S. DOE Office of Science Facility. The authors thank Michael Wörle and Reinhard Nesper for helpful discussions.

References

(1) C. G. Granqvist, *Sol. Energy Mater. Sol. Cells* **2000**, *60*, 201.

(2) Z.-F. Huang, J. Song, L. Pan, X. Zhang, L. Wang, J. Zou, *Adv. Mater.* **2015**, *27*, 5309.

(3) S. K. Deb, *Sol. Energy Mater. Sol. Cells* **2008**, *92*, 245.

(4) C. Janáky, K. Rajeshwar, N. R. de Tacconi, W. Chanmanee, M. N. Huda, *Catal. Today* **2013**, *199*, 53-64.

(5) H.B. Krause, W. G. Moulton, and R. C. Morris, *Acta Crystallogr., Sect. B* **1985** *41*, 11.

(6) M. Sato, B. H. Grier, G. Shirane, and H. Fujishita, *Phys. Rev. B* **1982**, *25*, 501.

(7) R. Brusetti, P. Haen, and J. Marcus, *Phys. Rev. B* **2002**, *65* 144528.

(8) D. Hirai, M. Bremholm, J. M. Allred, J. Krizan, L. M. Schoop, Q. Huang, J. Tao, and R. J. Cava, *Phys. Rev. Lett.* **2013**, *110*, 166402.

(9) M. Greenblatt (1996) Molybdenum and Tungsten Bronzes. In: C. Schlenker, J. Dumas, M. Greenblatt, S. van Smaalen (eds) Physics and Chemistry of Low-Dimensional Inorganic Conductors. NATO ASI Series (Series B: Physics), vol 354. Springer, Boston, MA.

(10) M. Greenblatt, *Acc. Chem. Res.*, **1996**, *29*, 219.

(11) Y. Ikeuchi, H. Takatsu, C. Tassel, Y. Goto, T. Murakami, H. Kageyama *Angew. Chem. Int. Ed.* **2017**, *56*, 5770.

(12) M. Parmentier, C. Gleitzer, and A. Coutoise, *Mater. Res. Bull.*, **1975**, *10*, 341.

(13) M. Parmentier, and C. Gleitzer, *C.R. Acud. Sci. Sér C*, **1975**, *281*, 819.

(14) S. T. Triantafyllou, P. C. Christidis, and C. B. Lioutas, *Journal of Solid State Chemistry*, **1997**, *134*, 344.

(15) M. Klingstedt, M. Sundberg, L. Eriksson, S. Haigh, A. Kirkland, D. Grüner, A. De Backer, S. van Aert, and O. Terasaki, *Z. Kristallogr.*, **2012**, *227*, 341.

(16) C. Parmentier, C. and Gleitzer, *Acta Cryst. B*, **1979**, *35*, 1963.

(17) F. Montilla, E. Morallon, A. De Battisti, S. Barison, S. Daolio, and J. L. Vazquez *J. Phys. Chem. B* **2004** *108*, 15976.

(18) F. O. von Rohr, H. Ji, F. A. Cevallos, T. Gao, N. P. Ong, and R. J. Cava, *J. Am. Chem. Soc.*, **2017**, *139*, 2771.

(19) H. Takagi, B. Batlogg, H. L. Kao, J. Kwo, R. J. Cava, J. J. Krajewski, and W. F. Peck, *Physical Review Letters*, **1992**, *69*, 2975.

(20) F. von Rohr, R. Nesper, and A. Schilling, *Phys. Rev. B*, **2014**, *89*, 094505.

(21) D. C. Johnston, *J. Low Temp. Phys.*, **1976**, *25*, 145.

(22) N. Haldolaarachchige, Q. Gibson, J. Krizan, and R. J. Cava, *Phys. Rev. B*, **2014**, *89*, 104520.

(23) R. Brusetti, P. Haen, and J. Marcus, *Phys. Rev. B*, **2002**, *65*, 144528.

(24) J. D. Bocarsly, D. Hirai, M. N. Ali, and R. J. Cava, *Euro Phys. Lett.*, **2013**, *103*, 17001.

(25) D. Hirai, F. von Rohr, and R. J. Cava, *Phys. Rev. B.*, **2012**, *86*, 100505(R).

(26) H.R. Shanks, *Solid State Commun.*, **1974**, *15*, 753.

(27) D. J. Singh, and L. Nordstrom, *Planewaves, Pseudopotentials, and the LAPW Method*; Springer Science & Business Media: New York, 2006.

(28) G. K. H. Madsen, P. Blaha, K. Schwarz, E. Sjöstedt, and L. Nordström, L. *Phys. Rev. B* **2001**, *64*, 195134.

(29) E. Sjöstedt, L. Nordström, and D. Singh, *Solid State Commun.* **2000**, *114*, 15.